RSC Advances

PAPER

View Article Online
View Journal | View Issue

Cite this: *RSC Adv.*, 2017, **7**, 39024

Hydrothermal fabrication of reduced graphene oxide/activated carbon/MnO_2 hybrids with excellent electrochemical performance for supercapacitors

Yue Li, Lanshu Xu, Jianmin Gao and Xiaojuan Jin*

Received 25th June 2017
Accepted 27th July 2017

DOI: 10.1039/c7ra07056j

rsc.li/rsc-advances

A graphene/activated carbon/MnO_2 (GAM) composite was synthesized by reacting in a hydrothermal synthesis reactor and maintaining at 140 °C for 2 h. MnO_2 anchored on graphene/activated carbon (GR/AC) sheets and the activated carbon (AC) particles distributed on the graphene (GR) surface provided numerous meso/micropores that act as active sites for the discharge reaction. The GR forms a three-dimensional network with excellent electrical conductivity for application. In this study, we focus on the mass ratio of GR/AC and MnO_2. The test outcome indicated that the GAM electrodes displayed exceptionable electrochemical performances especially when the mass ratio of GR/AC and MnO_2 is 2 : 3. The specific capacitance of GAM has achieved 378 F g^{-1} at a constant current density of 50 mA g^{-1} in the 7 M KOH electrolytic solution. Beyond that, the GAM 2 : 3 electrodes have also shown splendid cyclic ability with a 91.58% capacitance retention over 3000 circles. The three dimensional network structure is expected to represent a thrilling orientation for heightening the electrochemical property of MnO_2 and could be generalized for projecting next-generation superior supercapacitors.

1. Introduction

Supercapacitors, also considered a unique class of energy storage, are obtaining renewed interest as fungible and supplemental technologies, which exhibit a high power density, long lifespan cycle, simple operation and fast charging and discharging capability,[1] with a series of utilizations from slightly electronic devices, and storage standby systems, to gas-electric hybrids and commercial scale energy and power resources management.[2] According to the charge-storage mechanisms, supercapacitors are commonly divided into double electric layer capacitors (DELCs), in which the capacitance arises from the separated electric charges between the electrolytic solution and the surface of the solid state electrode, and pseudocapacitors in which the capacitance is based on an electrochemically reversible and rapid faradic reaction taking place at the interface of the electrode/electrolyte solution.[3] DELCs are universally realized for a fast charging and discharging capability, excellent rate performance and long lifespan cycle. However, the low energy density is the primary challenge for the DELCs owing to the storing or releasing of charge relying only on physically absorbing or desorbing ions at the surface of electrode and the interface of electrolytic solution.[4] Carbon-based materials, for instance, AC and graphene, are commonly used as electrode materials for DELCs. Pseudocapacitors could increase enormously the energy density due to store charge by a chemical redox reaction on the superficies of the electrode. However, it is a significant challenge to enhance the cycling stability and power density simultaneously.[5] Metal oxides, such as MnO_2, are their representatives. Accordingly, the creation of polymer based equipment is a wise method to settle these impediments.[6] Pseudocapacitive transition metal oxides, for instance, MnO_2, RuO_2 and Co_3O_4, have been researched extensively as electrode materials for supercapacitors. MnO_2 is an extensively employed material owing to its low cost, excellent energy densities, environmental friendliness and plentifulness.[7] However, because of its low electrochemical performance (10^{-5}–10^{-6} S cm^{-1}), MnO_2 has a poor rate capability and instability for excellent power properties, which hinder its extensive utilization in energy storage systems.[8]

To enhance the electrochemical performance of carbon-based electrodes for perfecting electrochemical properties, lots of endeavors have been focused on the synthesis of GR/AC (carbon nanotubes) composites owing to their outstanding electrochemical performance. Generally, in the GR/AC composite, the GR forms a three-dimensional network with excellent electrical conductivity, while the AC particles on the GR surface provide numerous meso/micropores that act as active sites for the discharge reaction.[9] For GR/AC composites,

MOE Key Laboratory of Wooden Material Science and Application, Beijing Key Laboratory of Lignocellulosic Chemistry, MOE Engineering Research Center of Forestry Biomass Materials and Bioenergy, Beijing Forestry University, 35 Qinghua East Road, Haidian, 100083, Beijing, China. E-mail: jxj0322@163.com; Tel: +86 13718160441

Chao Zheng *et al.* have prepared GR/AC nanoscale hybrids with an excellent property as electrodes for supercapacitors. They found that very porous ACs adhere to the GR to constitute a wrinkled nanosheet structure which has exhibited specific capacitance up to 210 F g^{-1} and 103 F g^{-1} in an aqueous electrolytic solution and an organic electrolytic solution, respectively, which indicates that the porous GR/AC composite can be applied for high performance supercapacitors.[10] Lei Jiang *et al.* synthesized glucose-derived GR/AC composites. They investigated the effect of the mass ratio of GR in the precursor on the electrochemical performance of the composites as electrode materials for electrochemical capacitors. They also found that the thermal graphene oxide sheets serves as a winkled carrier to support the AC particles after activation.[11] Yao Chen *et al.* found a method of chemical activation with KOH to significantly increase the specific surface area of 798 m^2 g^{-1}. The specific capacitance and the energy density of the as-abstained GR/AC hybrid have achieved 122 F g^{-1} and 6.1 W h kg^{-1} in an aqueous electrolytic solution.[12] In our previous work, we prepared the GR/AC composites by pre-carbonization of the precursors and KOH activation of the pyrolysis products. The GR/AC electrode achieved a specific capacitance of 265 F g^{-1} under a current density of 50 mA g^{-1} in a 7 M KOH electrolytic solution.[9] To date, substantial endeavor has been thrown into designing innovative hybrids, developing structure majorization, and enhancing the electrochemical performances of carbon-based composite supercapacitors. However, it is a formidable task to improve the high conductivity and enhance capacitance simultaneously for the carbon-based composite supercapacitors because of their poor energy density as storing or releasing the charge only depends on physically absorbing or desorbing ions at the electrode and electrolytic solution interface.[13] Consequently, it is essential to design fancy hybrid electrodes through combining many functional guests into the carbon-based composite to enhance the specific capacitance and ameliorate efficiencies.[14]

MnO_2 has received especial interest for application in pseudocapacitors due to its low cost, wide potential window, environmental friendliness and high theoretical specific capacitance.[15] However, MnO_2's electrochemical performance is impeded owing to its low electrical conductivity, strong causticity of alkaline solution and differential active utilization.[16] MnO_2 nanoparticles could be integrated with electrical conductive substrates, such as carbon-based materials (graphene, activated carbon and carbon nanotubes) to perfect its low conductivity and active utilization.[17] Liu's group has prepared MnO_2/$MnCO_3$/rGO hybrid nanostructures. The rod-like MnO_2 was built into the reduced graphene oxide by a facile strategy and demonstrated a high energy density of 17.8 W h kg^{-1} in a steady potential window of 0–1.6 V.[18] Charl J. Jafta and co-workers developed an asymmetric electrochemical device with MnO_2/GO nanocomposites by a hydrothermal reaction. The excellent electrochemical property of the MnO_2/GO nanocomposites, with a specific capacitance of 280 F g^{-1}, energy density of 35 W h kg^{-1} and power density of 7.5 kW kg^{-1} at a current density of 0.5 A g^{-1}, combined with the wonderful long cycle life, proved that this asymmetric electrochemical device has the capacity of being perfected as a business-like electrode system.[3]

Herein, we developed a simple chemical procedure for creating a kind of 3D compound of GR/AC/MnO_2 nanostructures for high performance electrochemical electrodes. By incorporating MnO_2 into holey GR/AC, the MnO_2–holey GR/AC ultracapacitors can be installed, which is anticipated to enhance the capacitance and conductivity of ultracapacitors. The crystallinity of the MnO_2 spreads over the GR/AC sheets to a certain extent and holds back the conglomeration of GR sheets owing to van der Waals' forces reciprocity bringing about plenty of procurable superficial area and fertile vesicular structure for accumulation energy.[19] However, in another respect, the GR sheets pose as a brilliant conductive substrate, which supplies the high superficial area for the distribution of nano-size MnO_2 particles.[20] The existence of GR with excellent electroconductibility is favorable to make uniform the distribution of MnO_2 and the electroconductivity of the hybrid electrode.[21] Besides, the special structural characteristics of the GR/AC/MnO_2 introduce structural robustness and durability and protect the stability of the skeleton in the electrolytic solution.[22] But, increasing the mass loading spread over the substrate and a valid domination of the MnO_2 films' thickness are still challenges to be overcome.[23] In this work, the electrochemistry performance of the as-obtained GAM samples with different proportions of MnO_2 are discussed. When the mass radio of GR/AC and MnO_2 is 2 : 3, the specific capacitance of the 2 : 3 electrode peaked at 378 F g^{-1} at a current density of 50 mA g^{-1} compared with the specific capacitance of GR/AC composites, which achieved 264 F g^{-1} at 50 mA g^{-1}. And the GAM 2 : 3 electrode equally showed outstanding cycle ability with a 91.58% capacitance retention over 3000 cycles. This may develop some ideas for the next generation energy storages.

2. Experimental

2.1 Materials

The waste particleboards were favorably offered by Beijing Jiahekailai Furniture and Design Company, which were gained during the process of furniture manufacturing containing 10% urea formaldehyde resin adhesive by mass. And other chemicals of analytical grade were purchased from Beijing Lanyi Chemical Reagent.

2.2 Preparation of AC/GR hybrids

Graphene oxide powder used in this work was obtained by chemical exfoliation of natural graphite following the modified Hummers' method and the AC was obtained from waste particleboards combined with urea formaldehyde resin adhesive as described in our previous work.[24] The experimental steps of the preparation of GR/AC composites were as follows: briefly, 0.5 g of obtained GR powder and 2.0 g of carbonization based on waste particleboard were firstly added into 10 mL of deionized water and then dispersed by ultrasonication with a power of 300 W for 15 min. After that, the KOH and GR/AC with a mass ratio of 3 was added into the dispersion mixture in the ice water

bath which kept the temperature of the mixture lower than 30 °C. After 24 h, the mixtures were then activated at a temperature of 800 °C and maintained for 60 min surrounded with nitrogen. The as-obtained porous GR/AC composites were flushed first with 0.5 M HCl aqueous solution and distilled water, sequentially, until the pH of the solution was up to 6–7. Finally, the porous GR/AC composites were dried at 105 °C in an oven maintained for 8 h.

2.3 Preparation of GR/AC/MnO_2 hybrids

The GR/AC composites were obtained by pre-carbonization of the precursors and KOH activation of the pyrolysis products as described elsewhere. The synthesis process for the GR/AC/MnO_2 composites is shown in Fig. 1. Briefly, 0.3225 g of GR/AC composite was added into aqueous solution. Simultaneously, 0.2343 g $KMnO_4$ and 0.3759 g $MnSO_4$ were dissolved in distilled water. The probable formation of MnO_2 can be described as the following chemical equation: $3MnSO_4 + 2KMnO_4 + 2H_2O \rightarrow 5MnO_2 + 2H_2SO_4 + K_2SO_4$. The mass ratio of the obtained MnO_2 and GR/AC is 1 : 1. Similarly, 0.3514 g $KMnO_4$ and 0.5638 g $MnSO_4$, 0.4686 g $KMnO_4$ and 0.7518 g $MnSO_4$, 0.7028 g $KMnO_4$ and 1.1276 g $MnSO_4$ were dissolved in distilled water. And the mass ratio of the obtained MnO_2 and GR/AC is, relatively, 2 : 3, 1 : 2, 1 : 3. The obtained samples are marked as GAM 1 : 1, GAM 2 : 3, GAM 1 : 2, and GAM 1 : 3. The GR/AC composite, $KMnO_4$ and $MnSO_4$ aqueous solutions were mixed, with ultrasonication for 60 min. Subsequently, the homogeneous composite was transferred to a 100 mL hydrothermal synthesis reactor and maintained at 140 °C for 2 h. The obtained GR/AC/MnO_2 composites were washed with distilled water. These GR/AC/MnO_2 composites were maintained at 105 °C in an oven for 8 h. Next, the as-obtained electrodes were coated onto a nickel foam substrate with a bench press at a pressure of 30 MPa and sandwiched in a stainless steel cell with a pressure of 180 MPa. The as-prepared electrodes were dried in an oven at 105 °C for over 4 h. The electrodes were weighed and two electrodes of identical weight were selected for the measurements. The capacitive performance of all the samples was investigated in 7 M KOH using two-electrode cells.

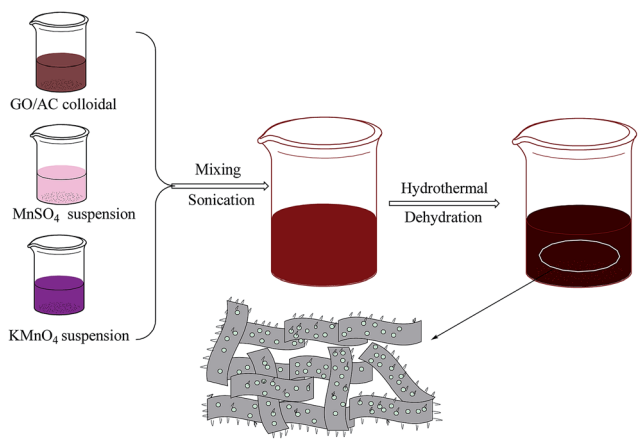

Fig. 1 Illustration of the fabrication process of GR/AC/MnO_2 composites.

2.4 Morphological and electrochemical analysis

The morphologies of the GR/AC/MnO_2 hybrids were investigated by scanning electron microscopy (SEM). Electrodes for the supercapacitors were prepared with the GR/AC/MnO_2 composites, acetylene black, and polytetrafluoroethylene (PTFE) with a mass ratio of 87 : 10 : 3. The electrochemical capacitive property of every hybrid sample was studied in a 7 M KOH electrolyte solution employing a two electrodes system (the electrode fabrication depended on our previous research). Galvanostatic charge–discharge, cyclic voltammetry, and alternating current impedance were adopted to evaluate the capacitance properties of the fabricated supercapacitor. Constant current density charge–discharge and rate performance were checked applying the BT2000 battery testing system (Arbin Instruments, USA) at room temperature. Cyclic voltammetry and alternating current impedance were employed in every sample for the electrochemical measurements using the 1260 electrochemical workstation (Solartron Metrology, UK) at room temperature.

3. Results and discussion

The morphologies of the GAM composites were observed by scanning electron microscopy (SEM) and the results of the experiments are described in Fig. 3. As shown in Fig. 3(a), the graphene as the substrate sustained the activated carbon particles. It also can be noticed in Fig. 3(b) and (c) that the MnO_2 maintained a nanoneedle coryneform and were closely anchored on the surface of GR/AC sheet and the interlayer. The GR is a thin sheet-like microstructure with folded portions. On the other hand, the growth of the MnO_2 on the interlayer also increased the layer spacing of graphene. The structure of the composite with MnO_2 growing on the GR/AC sheet is beneficial to the uniform dispersion of the MnO_2 and also promotes the separation of the graphene sheet. The structure can ensure a full contact of the MnO_2 and the highly conductive GR/AC and also improve the effective immersion of the electrolytic solution. Thereby, it can ensure the efficient transmission of electrons and ions as a supercapacitor electrode material. The surface morphology of the hybrids was also characterized by transmission electron microscopy (TEM). Fig. 3(d) describes the TEM image of the as-prepared GR/MnO_2 Fig. 3(e) and (f) show the TEM images of GAM. As shown in Fig. 3(e), the MnO_2 nanoparticles could be successfully prepared through a sample hydrothermal reaction and the MnO_2 nano-particles with an average diameter of 5–6 nm are closely anchored on the surface of the graphene. And the MnO_2 nanoparticles grew into a cluster, which looks like a loose sponge. Fig. 3(e) and (f) shows the GAM, with the homogeneous AC particles densely coated, which not only supplies an extra charge transmission route apart from the graphene floor but actively involves in the procedure of energy storage as both could be conductive to the charge storage of the entire layer through EDLCs and pseudocapacitance. To further understand the information of the process of MnO_2 anchored on GR/AC sheets, a probable mechanism is put forward according to the foundation of the

experimental results, as described in Fig. 2. As has been shown in our previous studies, GR sheets have their basal surface decked out mostly with epoxy and hydroxyl groups; nevertheless, carbonyl and carboxyl groups are mostly located on the edges of the GR sheets. These functional groups, acting as anchor sites, capacitate the subsequent *in situ* composition of nanostructures adhering to the surfaces and edges of GR sheets.[25] At the incipient stage, Mn^{2+} ions, formed by the dissolved solution of $MnSO_4$ in isopropyl alcohol, successfully combine with the negative charge of oxygen atoms containing functional groups on the GR/AC sheets through electrostatic forces. With the dropwise addition of $KMnO_4$ solution at room temperature, Mn^{2+} could be gradually oxidized into MnO_2 by $KMnO_4$. The MnO_2 will, through polymerization and further oriented growth along the GR/AC sheet, finally form MnO_2 ultrathin nanoflakes on the GR/AC sheet.[26] Besides, the GR/AC substrate can offer strong supporting networks for the orientation determination of the MnO_2 nanoflake growth. Besides, it also successfully prevents MnO_2 nanoflakes from self-assembly during the MnO_2 growth. This multichamber nanoflake structure is in favor of better contacting the electrode materials with the electrolytic solution, and offers a large area for the diffusion

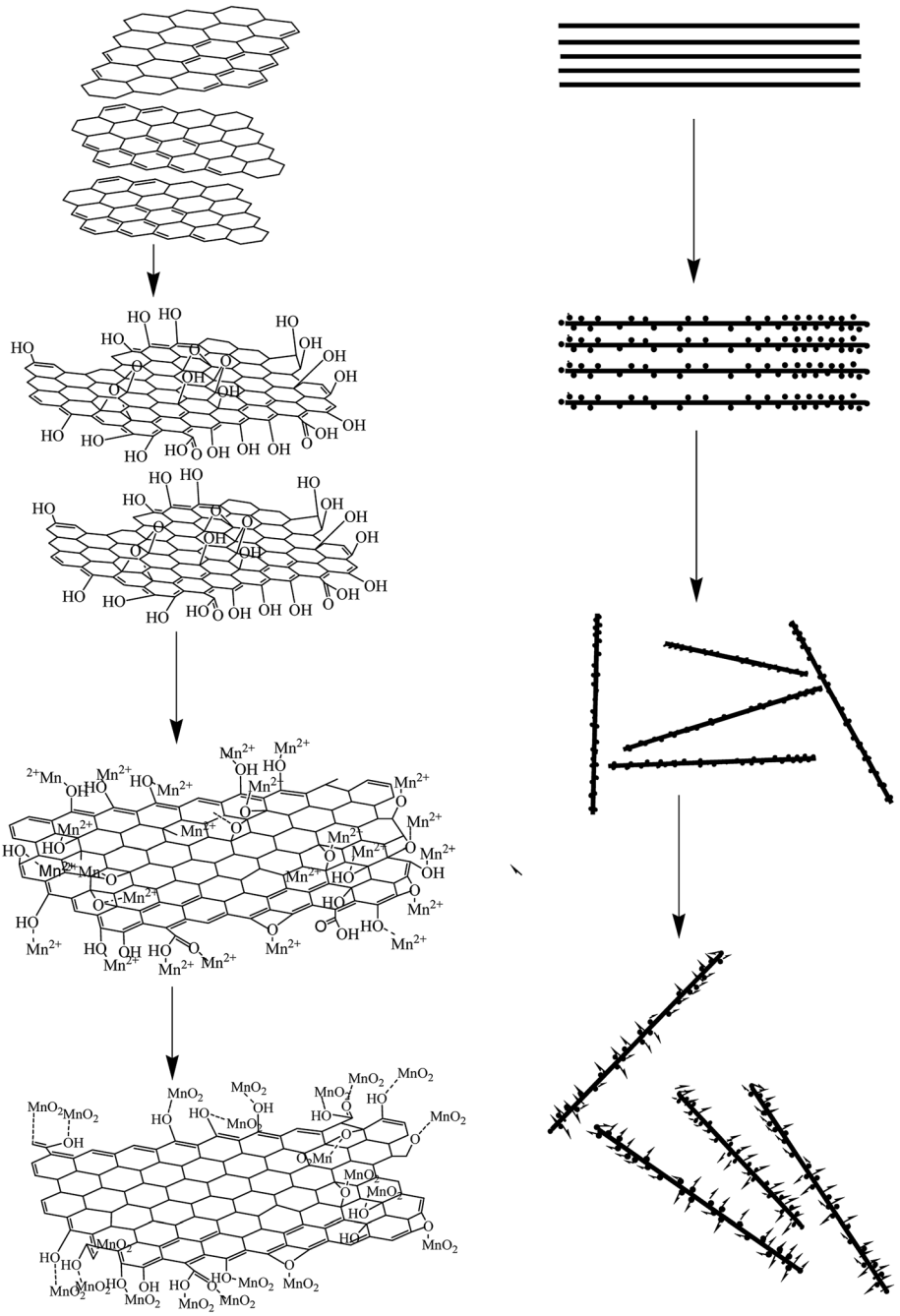

Fig. 2 Schematic illustration for the formation of the GR/AC/MnO_2 composite.

of ions and electronic transmission during the process of discharging and charging, and after that heightens the integral electrochemical properties.

The structural properties of the homo-nanostructured GR/AC and GAM hybrids were also characterized using Raman measurements. As described in Fig. 4(a), both spectra indicated the D and G bonds at ~1353 cm^{-1} and ~1592 cm^{-1}, respectively. For the GAM spectra, an Mn–O stretching vibration band at ~639 cm^{-1} could be observed, which could be attributed to the symmetric Mn–O stretching vibration of the MnO_6, further indicating the formation of MnO_2 in GAM.[27] The slightly higher intensity ratio of the D-bond to the G-bond (I_D/I_G) in GAM (1.25) compared to that of GR/AC (1.23) indicates that the deposition of MnO_2 on the GR/AC hybrids had a slight increase of the defect ratio and a negligible effect on the structure of the substrate.

The phase hybrids and crystal structures of the GR/AC and GAM composites were investigated by X-ray diffraction (XRD) patterns as described in Fig. 4(b). Two broad peaks at 2θ around 22° and 43° for the GR/AC hybrids are characteristic peaks of carbon-based materials,[28] which are in good agreement with the (002) and (101) crystal planes, respectively.[29] Three broad peaks at 12°, 37°, 55° and 66° appeared for the GAM hybrids, which could be indexed to the birnessite-type MnO_2. Furthermore, the peak at 2θ around 43° of the carbon-based materials disappeared after the deposition of MnO_2. This should be mainly attributed to the exfoliation of regular stacks of graphene oxides, which correlates well with the TEM image.

Fig. 5(a) describes the cyclic voltammetry curves (CVs) of the GR/AC, GAM 1 : 1, GAM 2 : 3, GAM 1 : 2, and GAM 1 : 3 electrodes in a 7 M KOH electrolytic solution at 50 mV s^{-1}. The potential window for cycling is confined between 0 V and 1.0 V. The CVs show a rectangular-like appearance and the GAM 2 : 3 electrode has the largest CV area, pointing out the GAM 2 : 3 electrode has the best capacitive performance. Comparing with the GR/AC electrode, the gravimetric current of GAM is very expensive due to the existence of pseudocapacitive MnO_2, which results in a higher gravimetric capacitance. Comparing with the GAM 1 : 1, GAM 2 : 3, GAM 1 : 2 and GAM 1 : 3, the GAM 2 : 3 electrode also displays the best capacitive performance, indicating that the GAM 2 : 3 electrode load is the most suitable amount of the MnO_2. When the quantity of MnO_2 is relatively less, the GR and AC in the composite can fully utilize the double layer energy storage. On the contrary, the amount of MnO_2 is sufficient, and the MnO_2 is densely covered on the surface and interlayer of the GR/AC and blocks the diffusion of the ions between the GR/AC, so that the surface utilization of GR/AC decreased and the capacitance is relatively low. Fig. 5(b) shows cyclic voltammograms of the GAM 2 : 3 electrode in a 7 M KOH electrolytic solution at different scan rates from 1 to 100 mV s^{-1}. The rate capability of the GAM 2 : 3 electrode is excellent, and it maintains an excellent rectangular CV appearance with only small tortuosity even at 100 mV s^{-1}. Under a scan rate of 100 mV s^{-1}, the GAM 2 : 3 electrode surrendered the largest current and resulted in a much higher capacitance, which is believed to be the collaborative function from every constituent of the combination electrode: GR backbone on the AC and the AC composed of individual particles that ultimately enlarge the electrical conductivity and administer to the redox-based pseudocapacitance.[30]

The galvanostatic charging and discharging curves of GAM 1 : 1, GAM 2 : 3, GAM 1 : 2, GAM 1 : 3 and GR/AC electrodes are explained in Fig. 5(c). In the charge/discharge procedure, the charge curves that are perfectly symmetric to its homologous discharge appropriate a trifling buckling, pointing out the pseudocapacitive dedication in connection with the contribution of the double layer.[31] In order to further understand the potential of the as-synthesized GAM 2 : 3 as an electrode

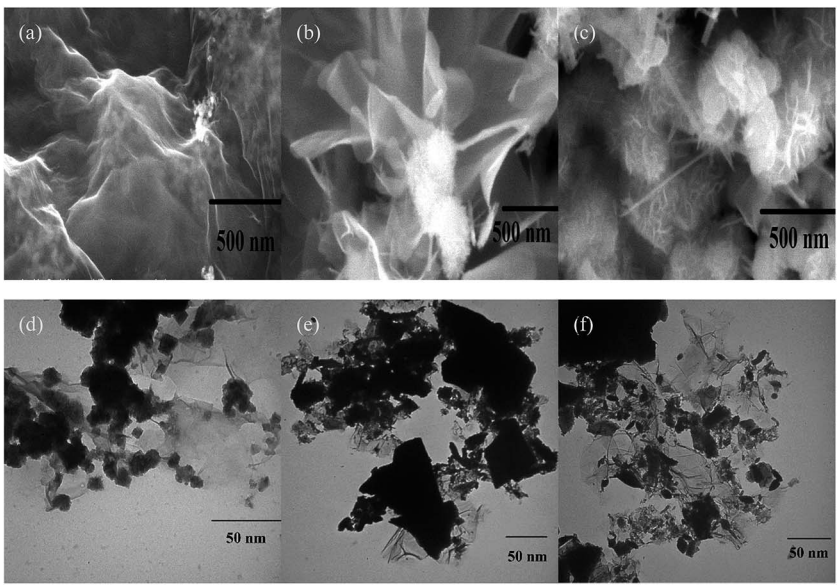

Fig. 3 SEM image of GR/AC and GAM samples: (a) SEM image of GR/AC. (b) and (c) SEM images of GAM. (d) TEM image of GR/MnO_2. (e) and (f) TEM images of GAM.

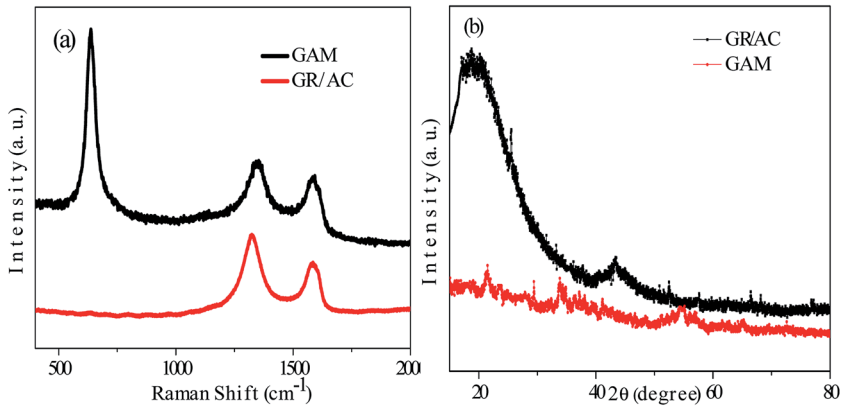

Fig. 4 (a) Raman spectra of GR/AC and GAM. (b) XRD patterns of GR/AC and GAM hybrids.

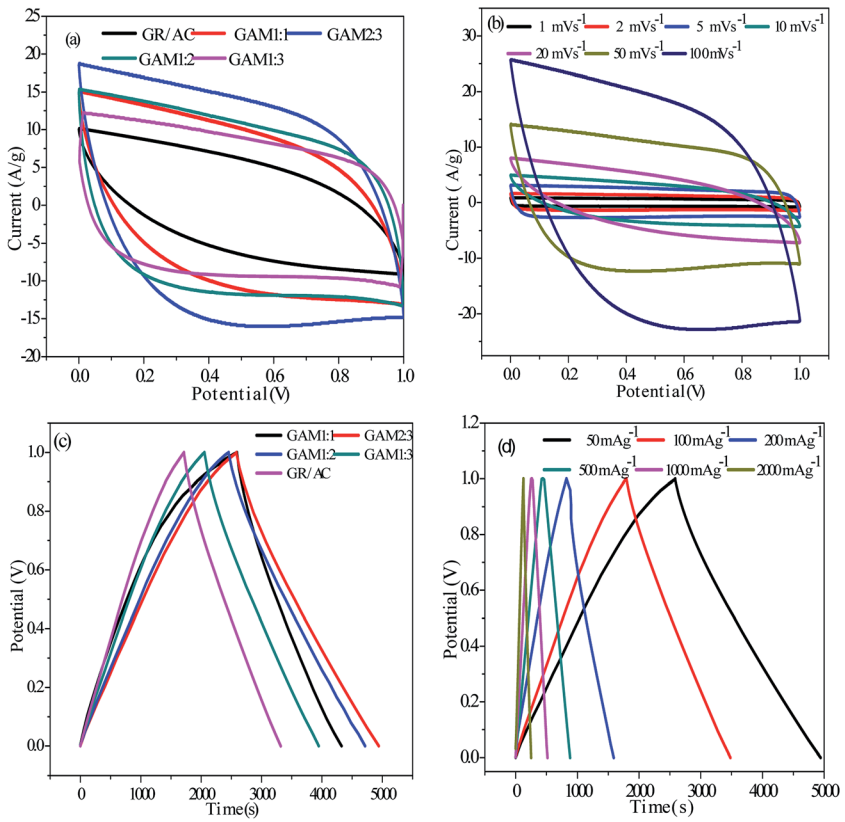

Fig. 5 (a) Cyclic voltammograms of the GR/AC, GAM 1 : 1, GAM 2 : 3, GAM 1 : 2 and GAM 1 : 3 electrodes in a 7 M KOH electrolytic solution at 50 mA s^{-1}. (b) Cyclic voltammograms of the GAM 2 : 3 electrode in a 7 M KOH electrolytic solution with different scan rates. (c) Galvanostatic charge–discharge curve of the GR/AC, GAM 1 : 1, GAM 2 : 3, GAM 1 : 2, and GAM 1 : 3 electrodes in a 7 M KOH electrolytic solution at a constant current density of 0.05 A g^{-1}. (d) Galvanostatic charge–discharge curve of the GAM 2 : 3 electrode in a 7 M KOH electrolytic solution at different constant current densities.

material for supercapacitors, galvanostatic charge/discharge measurements were also carried out in 7 M KOH between 0 and 1 V at different current densities from 50 mA g^{-1} to 2000 mA g^{-1} as shown in Fig. 5(d). It can be found that the charge curves are symmetrical to their corresponding discharge counterparts, which can strike a bargain with the CV curves. All the samples exhibit quasitriangular galvanostatic charge–discharge curves with great symmetry, even at 2 A g^{-1}, stating clearly preeminent capacitive properties and electrochemical invertibility. A small separation from the line in the work voltage–time curves relevant to the well-widened redox 'hump' in the galvanostatic charge/discharge curves[32] further evidences the existence of pseudocapacitance. The as-prefabricated GAM values of the supercapacitor are computed from the discharge curves based on the active hybrids on the entire two electrodes.

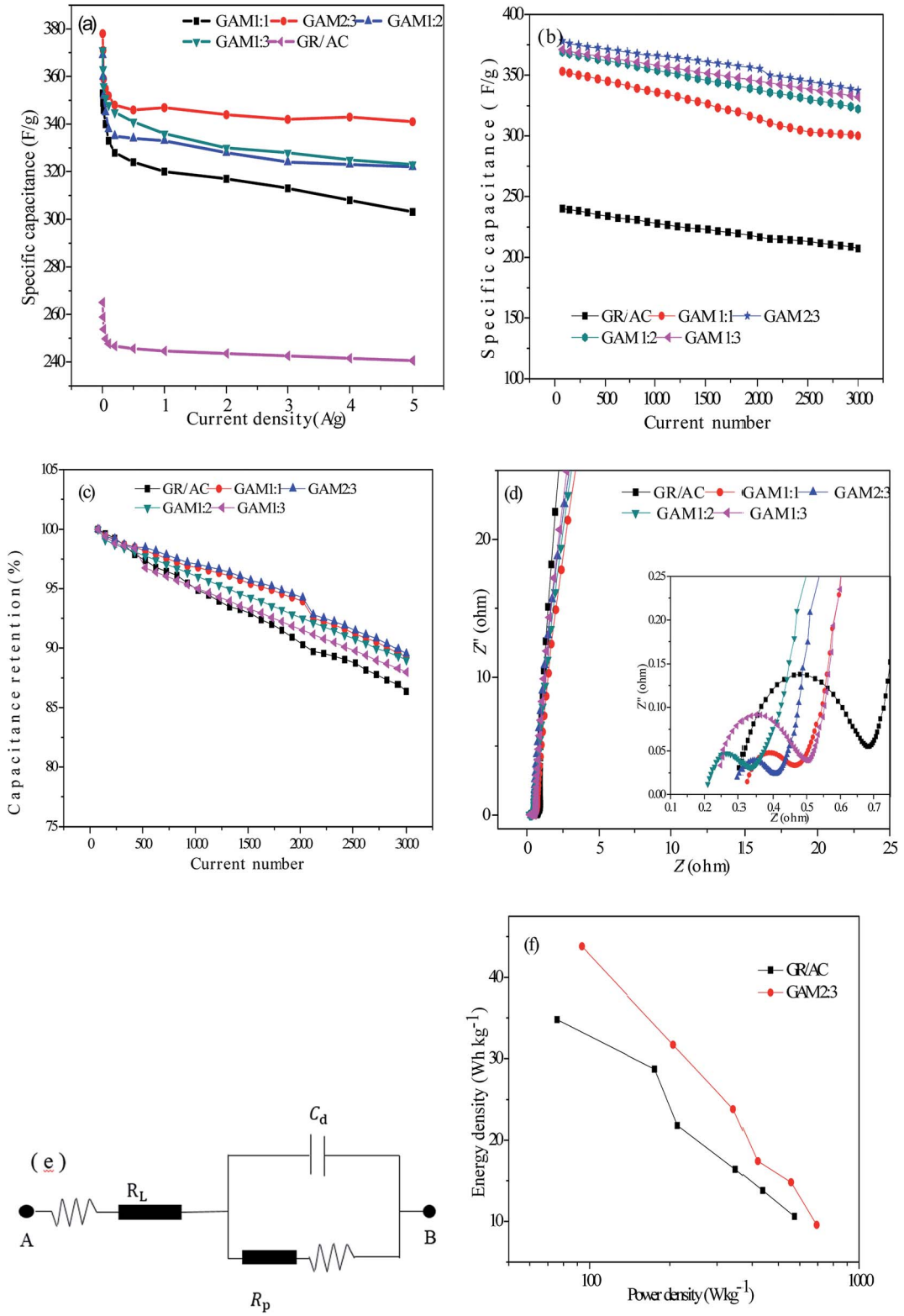

Fig. 6 (a) Capacitance and retention *versus* discharge current density from 0.05 to 5 A g^{-1} comparing GR/AC, GAM 1; 1, GAM 2 : 3, GAM 1 : 2, and GAM 1 : 3 electrodes. (b) Cycle life of the supercapacitor at a current density of 1.2 A g^{-1}. (c) The capacitance retention of the supercapacitor at a current density of 5 A g^{-1}. (d) Nyquist plot of the GR/AC, GAM 1 : 1, GAM 2 : 3, GAM 1 : 2, and GAM 1 : 3 electrodes in a 7 M KOH electrolytic solution over the frequency range from 0.01 Hz to 20 kHz. (e) The electrical equivalent circuit used for fitting impedance spectra. (f) The energy density and power density of GA and GAM hybrids supercapacitance.

Fig. 6(a) shows the relations between specific capacitance and charging and discharging current density to discuss the capacitance retention of all the electrodes. In our previous research, when the charging and discharging current density was increased from 50 to 2000 mA g^{-1}, the capacitance retention was still up to 92%, which indicates the as-synthesized samples are very appropriate for a higher current density application. Most weightily, it was also discovered that a high specific capacitance of 378 F g^{-1} can be achieved at 50 mA g^{-1}, which still maintains 343 F g^{-1} even at 5 A g^{-1}, which is more splendid than other electrodes, pointing out that the GAM 2 : 3 electrode holds the most qualified amount of the MnO_2. When the quantity of MnO_2 is relatively less, the MnO_2 is evenly distributed on the surface and interlayer of the GR/AC. And the GR/AC in the composite can fully utilize the double layer energy storage, and the surface, the internal holes and the layers can, as a device, store energy. On the other side, the GR/AC can play advantages of high conductivity and provide an efficient channel for the electron transport of MnO_2 and the double layer in the charging and discharging process. On the contrary, the amount of MnO_2 is sufficient, a part of the MnO_2 is difficult to come into contact with the highly conductive carbon material and the MnO_2 itself has poor conductivity since the surface of the graphene cannot provide enough nucleation sites, with the result that the electronic transmission is limited during the charge and discharge process. In addition, a large amount of MnO_2 also hinders the GR/AC substrate as a supercapacitor electrode material to play the role of double-layer storage, the ion is difficult to quickly embed and disengage in GR/AC to influence the charge storage. So the surface utilization of GR/AC decreases and the capacitance is relatively lower.

The specific capacitance of GR/AC/MnO_2 gradually decreased with the increase of current density, which could be ascribed to the low utilization efficiency of active materials under a high discharge current. Moreover, as shown in Fig. 6(b) and (c), the supercapacitor has a preeminent cycling stability with no palpable decline for the specific capacitance value in the first 1500 cycles and still maintains 91.58% of retention after 3000 circles. Such retention is superior as compared to the previously reported MnO_2-based supercapacitors, for instance GR/MnO_2 (~87% after 4000 cycles[33]), MnO_2/carbon nanofiber (~86.5% retention after 5000 cycles[34]).

EIS measurements were implemented to clarify the kinetics within the electrode, and equally to appraise the devotion of the MnO_2 to electrical double-layer capacitors in a frequency range of 0.1–10 kHz. The Nyquist plots for the GAM 1 : 1, GAM 2 : 3, GAM 1 : 2 and GAM 1 : 3 and GR/AC electrodes are shown in Fig. 6(d) and in Fig. 6(e) the electrical equivalent circuit used for fitting impedance spectra is shown. It is also approbatory that the inherent resistance of active materials could be figured out from the diameter of the semicircle in the high frequency region of Nyquist plots.[35] The EIS data were fitted by an equivalent circuit composed of a sum of the contact resistance and material resistance (R_L), a charge-transfer (R_P), a pseudocapacitive element (C_d) from the redox procedure of MnO_2, and a constant phase element (CPE) to account for the double-layer capacitance. R_L and R_P can be gained from the Nyquist plots, where the high frequency semicircle intercepts the real axis at R_L and (R_L + R_P), respectively. On the basis of this point, the material resistances (R_L) of the GAM 2 : 3 and GR/AC electrodes in the 7 M KOH electrolytic solution are 0.24 and 0.82, and the electrode of GAM 2 : 3 is evidently smaller than 0.82 of the GR/AC electrode, which is calculable from the value of the real axis. At the low frequency region, the slope reflects the diffusive resistivity of the electrolytic solution ions within the pores. The GAM 2 : 3 electrode exhibits a near vertical line which indicates ideal capacitive behavior. In contrast, the GR/AC electrode has a line that is slightly inclined from the ideal vertical line, which indicates a higher diffusive resistivity.

Fig. 6(f) shows the Ragone plots of the GA and GAM 2 : 3 hybrid electrodes that correspond to the energy densities and power densities with current densities ranging from 0.05 to 5 A g^{-1}. The energy density of GA is 34.8 W h kg^{-1} at a power density of 75.7 W kg^{-1}, and the energy density is 28.7 W h kg^{-1} at a power density of 175.7 W kg^{-1}. Compared with the GA hybrids, the GAM 2 : 3 hybrids exhibit an excellent electrochemical property with the energy density able to achieve 43.8 W h kg^{-1} at a power density of 93.7 W kg^{-1}, and the energy density also could be up to 31.7 W h kg^{-1} at a power density of 205.5 W kg^{-1}. Nevertheless, the energy density decreased with increasing power density, which is more excellent than other reported supercapacitance. Y. Chen and his co-workers successfully synthesized one-dimensional high graphitic carbon-tipped manganese oxide/mesoporous carbon/manganese oxide hybrid nanowires with energy densities achieved that can be as high as 20.8 W h kg^{-1}, at a power density of 30 W kg^{-1}.[12] Z.-L. Wu *et al.* has prepared manganese oxide/graphene oxide hybrids for high energy electrochemical capacitors with an energy density of 35 W h kg^{-1} at a power density of 7.5 W kg^{-1}.[19] Combining the advantages of a high specific capacitance, the simple fabrication method, and environmentally friendly nature and the high energy density demonstrates that the as-fabricated GMA hybrids for supercapacitance devices are very promising energy storage systems.

4. Conclusions

In summary, we have successfully synthesized GAM composites through a simple hydrothermal strategy. The obtained nanohybrids exhibited a highly conductive architecture in which MnO_2 anchored on the GR/AC sheets and the AC particles on the graphene surface provided numerous meso/micropores that act as active sites for the discharge reaction and the GR formed a three-dimensional network with an excellent electrical performance for application, endowing the composite with a high specific capacitance, and excellent rate capability and cycle stability. When the mass ratio of GR/AC and MnO_2 is 2 : 3, the specific capacitance achieved 378 F g^{-1} at 50 mV s^{-1} in the 7 M KOH electrolytic solution. Moreover, these composite electrodes have also exhibited excellent cycling performances with 91.58% capacitance retention over 3000 cycles. The 3D conductive wrapping structure is expected to represent an exciting direction for enhancing the electrochemical

performance of metal oxides and can be generalized for designing next-generation high-performance energy storage devices.

Acknowledgements

The authors gratefully acknowledge the financial support of National Natural Science Foundation, project 51572028: the study on the technology and mechanism of the activated carbon electrode from waste hard board.

References

1 J. Hong, Y.-W. Lee, D. Ahn, S. Pak, J. Lee, A.-R. Jang, S. Lee, B. Hou, Y. Cho and S. M. Morris, Highly Stable 3D Porous Heterostructures with Hierarchically-Coordinated Octahedral Transition Metals for Enhanced Performance Supercapacitors, *Nano Energy*, 2017, DOI: 10.1016/j.nanoen.2017.07.010.

2 S.-H. Li, Q.-H. Liu, L. Qi, L.-H. Lu and H.-Y. Wang, Progress in Research on Manganese Dioxide Electrode Materials for Electrochemical Capacitors, *Chin. J. Anal. Chem.*, 2012, **40**, 339–346.

3 C. J. Jafta, F. Nkosi, L. le Roux, M. K. Mathe, M. Kebede, K. Makgopa, Y. Song, D. Tong, M. Oyama, N. Manyala, S. Chen and K. I. Ozoemena, Manganese oxide/graphene oxide composites for high-energy aqueous asymmetric electrochemical capacitors, *Electrochim. Acta*, 2013, **110**, 228–233.

4 T.-X. Shang, R.-Q. Ren, Y.-M. Zhu and X.-J. Jin, Oxygen- and nitrogen-co-doped activated carbon from waste particleboard for potential application in high-performance capacitance, *Electrochim. Acta*, 2015, **163**, 32–40.

5 T. Chen and L. Dai, Carbon nanomaterials for high-performance supercapacitors, *Mater. Today*, 2013, **16**, 272–280.

6 K. H. Jeong, H. J. Lee, M. F. Simpson and S. M. Jeong, Electrochemical Synthesis of Graphene/MnO_2 Nano-Composite for Application to Supercapacitor Electrode, *J. Nanosci. Nanotechnol.*, 2016, **16**, 4620–4625.

7 S. Khilari, S. Pandit, M. M. Ghangrekar, D. Das and D. Pradhan, Graphene supported α-MnO_2 nanotubes as a cathode catalyst for improved power generation and wastewater treatment in single-chambered microbial fuel cells, *RSC Adv.*, 2013, **3**, 7902.

8 D. Wu, S. Xu, C. Zhang, Y. Zhu, D. Xiong, R. Huang, R. Qi, L. Wang and P. K. Chu, Three-dimensional homo-nanostructured MnO_2/nanographene membranes on a macroporous electrically conductive network for high performance supercapacitors, *J. Mater. Chem. A*, 2016, **4**, 11317–11329.

9 Y. Li, T.-X. Shang, J.-M. Gao and X.-J. Jin, Nitrogen-doped activated carbon/graphene composites as high-performance supercapacitor electrodes, *RSC Adv.*, 2017, **7**, 19098–19105.

10 C. Zheng, X. Zhou, H. Cao, G. Wang and Z. Liu, Synthesis of porous graphene/activated carbon composite with high packing density and large specific surface area for supercapacitor electrode material, *J. Power Sources*, 2014, **258**, 290–296.

11 L. Jiang, J. Yan, Y. Zhou, L. Hao, R. Xue, L. Jiang and B. Yi, Activated carbon/graphene composites with high-rate performance as electrode materials for electrochemical capacitors, *J. Solid State Electrochem.*, 2013, **17**, 2949–2958.

12 Y. Chen, X. Zhang, H. Zhang, X. Sun, D. Zhang and Y. Ma, High-performance supercapacitors based on a graphene–activated carbon composite prepared by chemical activation, *RSC Adv.*, 2012, **2**, 7747–7753.

13 Y. Lei, Z.-H. Huang, Y. Yang, W. Shen, Y. Zheng, H. Sun and F. Kang, Porous mesocarbon microbeads with graphitic shells: constructing a high-rate, high-capacity cathode for hybrid supercapacitor, *Sci. Rep.*, 2013, **3**, 2477.

14 P. Iamprasertkun, A. Krittayavathananon, A. Seubsai, N. Chanlek, P. Kidkhunthod, W. Sangthong, S. Maensiri, R. Yimnirun, S. Nilmoung and P. Pannopard, Charge storage mechanisms of manganese oxide nanosheets and N-doped reduced graphene oxide aerogel for high-performance asymmetric supercapacitors, *Sci. Rep.*, 2016, **6**, 37560.

15 Y. Zhao, W. Ran, J. He, Y. Huang, Z. Liu, W. Liu, Y. Tang, L. Zhang, D. Gao and F. Gao, High-performance asymmetric supercapacitors based on multilayer MnO_2/graphene oxide nanoflakes and hierarchical porous carbon with enhanced cycling stability, *Small*, 2015, **11**, 1310–1319.

16 T. Brousse, M. Toupin and D. Bélanger, A Hybrid Activated Carbon-Manganese Dioxide Capacitor using a Mild Aqueous Electrolyte, *J. Electrochem. Soc.*, 2004, **151**, A614.

17 Y. R. Chen, K. F. Chiu, H. C. Lin, C. L. Chen, C. Y. Hsieh, C. B. Tsai and B. T. T. Chu, Graphene/activated carbon supercapacitors with sulfonated-polyetheretherketone as solid-state electrolyte and multifunctional binder, *Solid State Sci.*, 2014, **37**, 80–85.

18 Y. Liu, D. He, H. Wu, J. Duan and Y. Zhang, Hydrothermal self-assembly of manganese dioxide/manganese carbonate/reduced graphene oxide aerogel for asymmetric supercapacitors, *Electrochim. Acta*, 2015, **164**, 154–162.

19 Z.-L. Wu, C.-K. Li, J.-G. Yu and X.-Q. Chen, MnO_2/reduced graphene oxide nanoribbons: facile hydrothermal preparation and their application in amperometric detection of hydrogen peroxide, *Sens. Actuators, B*, 2017, **239**, 544–552.

20 J. Yan, Z. Fan, T. Wei, W. Qian, M. Zhang and F. Wei, Fast and reversible surface redox reaction of graphene–MnO_2 composites as supercapacitor electrodes, *Carbon*, 2010, **48**, 3825–3833.

21 G. Yu, L. Hu, N. Liu, H. Wang, M. Vosgueritchian, Y. Yang, Y. Cui and Z. Bao, Enhancing the supercapacitor performance of graphene/MnO_2 nanostructured electrodes by conductive wrapping, *Nano Lett.*, 2011, **11**, 4438–4442.

22 Q. Yang, L. Dong, C. Xu and F. Kang, High-performance supercapacitors based on graphene/MnO_2/activated carbon fiber felt composite electrodes in different neutral electrolytes, *RSC Adv.*, 2016, **6**, 12525–12529.

23 Y. Liu, K. Shi and I. Zhitomirsky, Asymmetric supercapacitor, based on composite MnO_2-graphene and N-doped activated carbon coated carbon nanotube electrodes, *Electrochim. Acta*, 2017, **233**, 142–150.
24 C. Li and G. Shi, Functional gels based on chemically modified graphenes, *Adv. Mater.*, 2014, **26**, 3992–4012.
25 A. Davies and A. Yu, Material advancements in supercapacitors: from activated carbon to carbon nanotube and graphene, *Can. J. Chem. Eng.*, 2011, **89**, 1342–1357.
26 H. Lee, S. H. Park, S.-J. Kim, Y.-K. Park, B.-J. Kim, K.-H. An, S. J. Ki and S.-C. Jung, Synthesis of manganese oxide/activated carbon composites for supercapacitor application using a liquid phase plasma reduction system, *Int. J. Hydrogen Energy*, 2015, **40**, 754–759.
27 Y. Zhao, W. Ran, J. He, Y. Huang, Z. Liu, W. Liu, Y. Tang, L. Zhang, D. Gao and F. Gao, High-Performance Asymmetric Supercapacitors Based on Multilayer MnO_2/Graphene Oxide Nanoflakes and Hierarchical Porous Carbon with Enhanced Cycling Stability, *Small*, 2015, **11**, 1310–1319.
28 J. Zhou, J. Song, H. Li, X. Feng, Z. Huang, S. Chen, Y. Ma, L. Wang and X. Yan, The synthesis of shape-controlled α-MoO_3/graphene nanocomposites for high performance supercapacitors, *New J. Chem.*, 2015, **39**, 8780–8786.
29 Z. Jin, Q. Zhang, S. Yuan and T. Ohno, Synthesis high specific surface area nanotube gC3N4 with two-step condensation treatment of melamine to enhance photocatalysis properties, *RSC Adv.*, 2015, **5**, 4026–4029.
30 Y. Chen, Y. Zhang, D. Geng, R. Li, H. Hong, J. Chen and X. Sun, One-pot synthesis of MnO_2/graphene/carbon nanotube hybrid by chemical method, *Carbon*, 2011, **49**, 4434–4442.
31 J. Zhang, G. Wang, W. Wang, H. Song and L. Wang, Preparation of manganese dioxide loaded activated carbon adsorbents and their desulfurization performance, *Russ. J. Phys. Chem. A*, 2016, **90**, 2633–2641.
32 Z. Fan, J. Yan, T. Wei, L. Zhi, G. Ning, T. Li and F. Wei, Asymmetric Supercapacitors Based on Graphene/MnO_2 and Activated Carbon Nanofiber Electrodes with High Power and Energy Density, *Adv. Funct. Mater.*, 2011, **21**, 2366–2375.
33 M. F. Hossain and J. Y. Park, Plain to point network reduced graphene oxide-activated carbon composites decorated with platinum nanoparticles for urine glucose detection, *Sci. Rep.*, 2016, **6**, 21009.
34 R. Ranjusha, A. Sreekumaran Nair, S. Ramakrishna, P. Anjali, K. Sujith, K. R. V. Subramanian, N. Sivakumar, T. N. Kim, S. V. Nair and A. Balakrishnan, Ultra fine MnO_2 nanowire based high performance thin film rechargeable electrodes: effect of surface morphology, electrolytes and concentrations, *J. Mater. Chem.*, 2012, **22**, 20465.
35 H. Li, J. Song, L. Wang, X. Feng, R. Liu, W. Zeng, Z. Huang, Y. Ma and L. Wang, Flexible all-solid-state supercapacitors based on polyaniline orderly nanotubes array, *Nanoscale*, 2017, **9**, 193–200.